Original Article

Institution of MECHANICAL ENGINEERS
Journal of MULTI-BODY DYNAMICS

Proc IMechE Part K:
J Multi-body Dynamics
0(0) 1–16

DOI: 10.1177/1464419314528319
pik.sagepub.com
SAGE

Methods of modeling slope discontinuities in large size wind turbine blades using absolute nodal coordinate formulation

AH Bayoumy[1], AA Nada[2] and SM Megahed[3]

Abstract

This paper describes and evaluates the use of the Absolute Nodal Coordinate Formulation (ANCF) in modeling large size wind turbine blades. Modern blade model can be divided into two regions classified by aerodynamic and structural function. The aerodynamic region, blade-span, is utilizing the thinnest possible airfoil section. On the other hand, the transition between the circular mount and the first airfoil profile is referred as blade-root region, which carries highest loads along the blade. In this investigation, an efficient procedure is developed for mapping NACA airfoil wind-turbine blades into ANCF thin plate models. The procedure concerns a complete wind turbine blade structure, blade-root as well as the blade-span regions with non-uniform and twisted nature. As a result, the slope discontinuity problem arises in both chord-wise and span-wise directions, and consequently presents numerical errors in dynamic simulation. The paper investigates the methods of modeling slope discontinuity resulting from the variations of the cross-sectional layouts across the blade. The developed method is applied for the gradient-deficient thin plate element in order to account for structural discontinuity. In addition, the aerodynamic loads are precisely expressed and the aerodynamic characteristics of such blades are examined with the ANCF and with the classical finite element method. The static and dynamic solutions of different operating conditions are obtained and results are compared with those obtained using ANSYS code. Both the limitations and advantages of using the ANCF in modeling large size wind turbine blades are concluded and discussed. A Dynamics for Design (DFD) procedure is presented with numerical example concerning large-rotation, large deformation wind turbine blades.

Keywords

Absolute nodal coordinate formulation, wind turbine blade, plate element, large rotation, large deformation

Date received: 18 November 2013; accepted: 25 February 2014

Introduction

Wind turbines are designed to exploit the wind energy that exists at certain locations. The rotor (includes blades) is approximately 20% of the wind turbine cost, which converts wind energy to low speed rotational energy.[1] The wind turbine blade is the main element that interacts with wind, and the energy capture increases with the length of the blades.[2] The size of commercial wind turbines has increased dramatically in the last 25 years from approximately a rated power of 50 KW and a rotor diameter of 10–15 m up to 5 MW with a rotor diameter of more than 120 m.[3] The largest wind turbine, manufactured by the German wind turbine producer Enercon is shown in Figure 1, with a hub height of 135 m and rotor diameter of 127 m; this large model can generate up to 7.58 MW of power per turbine.[4]

Wind turbines are subjected to several operational scenarios: Normal, emergency stop and extreme loading during operation. In the case of large size wind turbine blades, the mass of the blade is said to increase proportionally at a cubic rate.[5] The gravitational and centrifugal forces become critical due to blade mass. Gyroscopic loads result from yawing during operation. Consequently, the load magnitude depends on the operational scenario under analysis as well as the system parameters (flexibility of blade, pitching, yawing and the generator connection). To counteract the weight increase, the development of blades goes towards long and relatively flexible structures. It is obvious that the design process of such large size should be based on accurate dynamic modeling of such blades and precise models of

[1]Power Generation Eng. and Services (PGESCo), Cairo, Egypt
[2]Benha Institute of Technology, Benha University, Benha, Egypt
[3]Egypt-Japan University of Science and Technology (E-JUST), New Borg El-Arab City, Alexandria, Egypt

Corresponding author:
AA Nada, Benha University, Benha, Egypt.
Email: arobust@tedata.net.eg

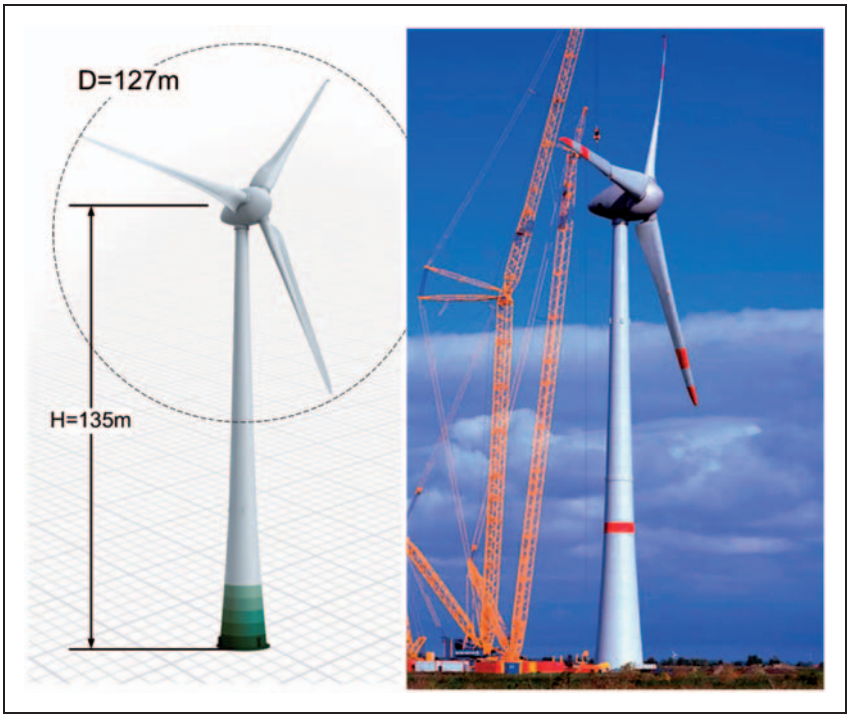

Figure 1. Large size wind turbine.[4]

aerodynamic loads. Furthermore, the dynamic model will be used for analysis, identification, and monitoring process.

It is found that the incremental finite element method can be used in modeling wind turbine blades in case of relatively flexible blades (small deformations), for buckling loads, transversal mode shapes and frequencies, see Hansena et al.[6] In the case of long and very flexible blades (large deformation) and extreme loading (large rotation) problems, the higher frequency modes cannot be ignored.[7] Furthermore, these high frequency modes cannot be computed by classical finite element due to its incremental nature. In this case, i.e., large deformation and large rotation case, the Absolute Nodal Coordinate Formulation (ANCF) is most suited method for modeling in order to capture the high frequency modes of the rotating blades.[8] The main advantage of using ANCF formulation in multibody computer simulations is that the resulting mass matrix is constant. This matrix enables to use non-incremental solution procedures in a general framework of multibody computer algorithms. The elastic forces, in contrast, are calculated using a general continuum mechanics approach that allows for describing the cross-section deformation modes as well as the deformation modes that appear in the existing beam theories. Recent advances in ANCF, involving the method of calculating the strain energy,[9,10] illuminating high frequency modes,[7,11] and development of stiff integrators,[12,13] help in reducing the calculation time and enhance the sensitivity of the system equations. Also, the formulation of 3D joint constraints is well established and verified,[14] which enables to construct the model of complete wind turbine blades and structure. Further advances in the ANCF are carried out including the modeling of internal damping,[15] nonlinear viscoelasticity[16] and piezoelectric laminates.[17] The main goal of this work is to give the answer of why/why not the ANCF is suited for modeling large size wind turbine blade application.

In the case of modeling wind turbine blades, the blade can be divided into two main areas classified by structural and aerodynamic functions. The first area is the blade-root, which is the transition between the circular mount and the first airfoil profile. This section carries the highest load with low aerodynamics efficiency. The second area is the blade-span, which is aerodynamically significant and therefore the thinnest possible airfoil section is utilized. In Nada,[8] the ANCF is used for constructing a continuum model of blade-span with uniform structure, in this model, Bspline surface is used to approximate airfoil structures. In Bayoumy et al.,[18] the ANCF is used in modeling the blade-span for non-uniform and twisted structure; in this model, an analytical and explicit procedure is established for calculating the ANCF positions and gradients of NACA (National Advisory Committee for Aeronautics airfoils). Both models concern the ANCF thin plate element for modeling the blade-span structure due to its aerodynamical nature. The use of the thin plate element is more efficient in that application because of the relative scale between the thickness and length and width.

Because of the variations of the cross-sectional layouts across the blade, structural discontinuities are found between the upper and lower surfaces (chordwise slope discontinuity) and between the blade body

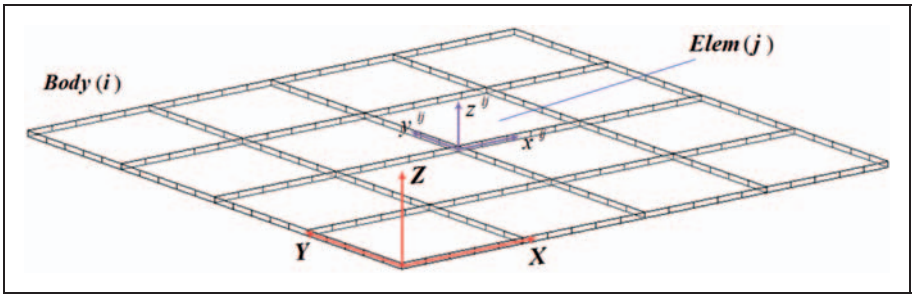

Figure 2. Undeformed configuration of plate element.

and root section (span-wise slope discontinuity). Methods of modeling slope discontinuities in ANCF of wind turbine blade are carried out in Bayoumy et al.[19] In Bayoumy et al.,[19] methods of modeling slope discontinuities are illustrated and examined under gravitational loads of the blade. In this case, the deformation is relatively small and the structural behavior of the blade is examined under small deformation case.

In this paper, the complete model of the wind turbine blade (root and span sections) is carried out. The methods of modeling slope discontinuities are presented in such a way to avoid coordinates redundancy, and the obtained blade models are illustrated. On the other hand, the aerodynamic loads are precisely expressed and the aerodynamics characteristics of wind blades are examined for different operating conditions. These conditions include the normal and full-feathered operating condition (braking condition), in which the transverse deformation is maximum. The simulation results are compared with ANSYS code.[20] Based on the numerical results, the advantages of using the ANCF in modeling large size wind turbine blades are concluded with respect to classical finite element methods.

ANCF model of wind turbine blades

Modern blade model can be divided into two regions classified by aerodynamic and structural function. The aerodynamic region, blade-span, is utilizing the thinnest possible airfoil section. However, the transition between the circular mount and the first airfoil profile is referred as the blade-root region, which carries highest loads along the blade. An efficient procedure is developed in Bayoumy et al.[18,19] for mapping NACA airfoils of wind-turbine blades into ANCF thin plate models. It concerns complete wind turbine blade structure, blade-root as well as the blade-span regions with non-uniform and twisted nature. This procedure includes explicit forms of the nodal positions and the associated gradients of 12 thin plate elements to construct the blade model. In Bayoumy et al.,[18] several sections along the blade-span shows more accurate results for the blade-span dynamics characteristics compared with ANSYS code. One major problem that appears in the case of complete wind turbine structure is the slope discontinuity problem, which arises in both the chord-wise and span-wise directions, and consequently presents numerical errors in dynamic simulation. Bayoumy et al.[19] investigated the methods for modeling slope discontinuity resulting from the variations of the cross-sectional layouts across the blade. The developed method is applied for the gradient-deficient thin plate element in order to account for structural discontinuity. In this section, the ANCF model of large size wind turbine blade is presented and the method used for modeling structural discontinuity is illustrated.

Absolute nodal coordinate formulation

In the ANCF, the nodal coordinates of the elements are defined in a fixed inertial coordinate system, and this fixed inertial coordinate system should be mentioned here as the Structure Coordinate System **SCS:**(XYZ). The nodal coordinates of an element j consist of the global displacements and slopes of each node. For a 4-noded plate element, element j, on body i, as shown in Figure 2, the nodal coordinates of node k, $k=(1, 2, 3, 4)$ can be written as[21]

$$\mathbf{e}^{ijk} = \left[\mathbf{r}^{ijk^T} \quad \frac{\partial \mathbf{r}^{ijk^T}}{\partial x^{ij}} \quad \frac{\partial \mathbf{r}^{ijk^T}}{\partial y^{ij}} \quad \frac{\partial \mathbf{r}^{ijk^T}}{\partial z^{ij}} \right]^T \tag{1}$$

where $\mathbf{r}^{ijk}$ defines the global position of node k and the three vectors $\partial \mathbf{r}^{ijk}/\partial x^{ij}$, $\partial \mathbf{r}^{ijk}/\partial y^{ij}$, and $\partial \mathbf{r}^{ijk}/\partial z^{ij}$, define the position vector gradients at node k with respect to the element coordinate system **ECS:** $\left(x^{ij}, y^{ij}, z^{ij}\right)$. As a consequence, such a representation guarantees inter-element continuity of global displacement gradients at these points. The nodal coordinates of one element can then be given by the vector $\mathbf{e}^{ij} = \left[\mathbf{e}^{ij1T} \quad \mathbf{e}^{ij2T} \quad \mathbf{e}^{ij3T} \quad \mathbf{e}^{ij4T} \right]^T$. In the ANCF, the global position of an arbitrary point on the body i, element j, is defined as

$$\mathbf{r}^{ij} = \mathbf{S}^{ij}\left(\mathbf{x}^{ij}\right)\mathbf{e}^{ij} \tag{2}$$

where $\mathbf{S}^{ij}$ is the element shape function matrix,[21] $\mathbf{x}^{ij} = \left[x^{ij} \quad y^{ij} \quad z^{ij} \right]^T$ is the local position of the

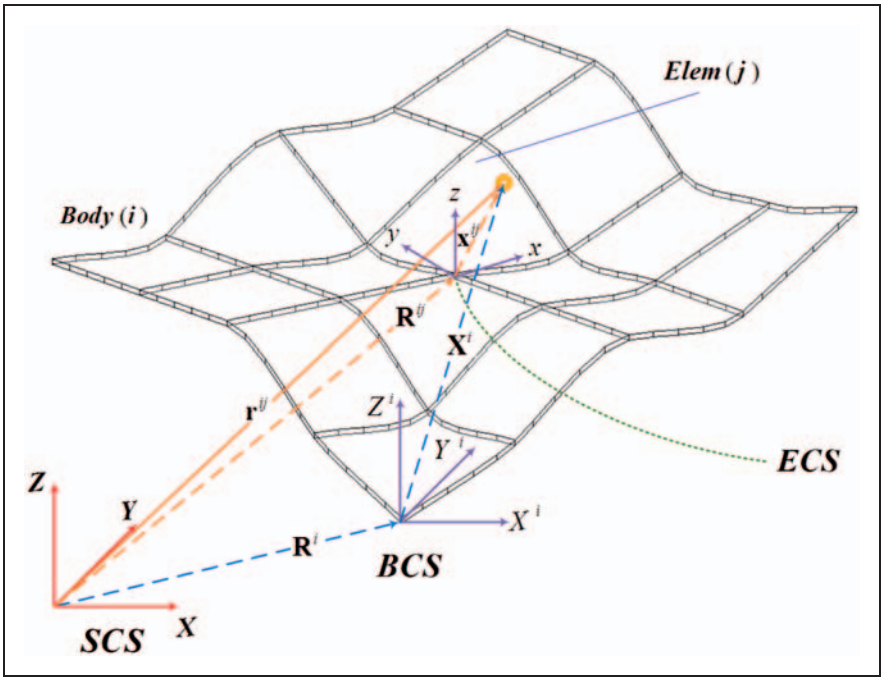

Figure 3. Structure (SCS), body (BCS), and element (ECS) coordinate systems of continuous structure.

point, x^{ij}, y^{ij}, and z^{ij} are the local coordinates of the element defined in the **ECS.** By defining $\mathbf{p}^i$ as the *unconstrained* vector of nodal coordinates over the flexible body i, with the dimension of $DOFs \times 1$, where $DOFs$ are the total number of degrees of freedom, equation (2) can be rewritten as

$$\mathbf{r}^{ij} = \mathbf{S}^{ij}\mathbf{e}^{ij} = \mathbf{S}^{ij}\mathbf{B}_1^{ij}\mathbf{B}_2^i\mathbf{p}^i \tag{3}$$

where $\mathbf{B}_1^{ij}$ is the connectivity matrix and $\mathbf{B}_2^i$ is boundary conditions linear-transformation matrix.

In the case of element which has an arbitrary initial orientation, see Figure 3, $\mathbf{r}^{ij}$ can be defined using the **ECS** as follows

$$\mathbf{r}^{ij} = \mathbf{R}^{ij} + \mathbf{A}^{ij}\mathbf{x}^{ij} \tag{4}$$

where $\mathbf{R}^{ij}$ is the global position vector of the origin of the element coordinate system, and $\mathbf{A}^{ij}$ is the transformation matrix that defines the orientation of the **ECS** with respect to the **SCS**. Therefore, the position vector gradients with respect to the **ECS** in the initial configuration can be obtained as

$$\frac{\partial \mathbf{r}^{ij}}{\partial \mathbf{x}^{ij}} = \mathbf{A}^{ij} \tag{5}$$

To maintain the desirable features of the ANCF that include a constant mass matrix and zero Coriolis and centrifugal forces, it is provided that all the element transformation matrices that define the orientation of the **ECS** with respect to **SCS** are the same. That is if two elements have initially different orientations, the continuity of the position vector gradients cannot be maintained and, consequently, this leads to a nonlinear mass matrix for the flexible body. In order to counteract this problem, an intermediate coordinate system is introduced and mentioned by the body coordinate system **BCS**.[22] If the axes of the **BCS** are selected to be initially parallel to the axes of the **SCS**, as shown in Figure 3, equation (4) should take the form of

$$\mathbf{r}^{ij} = \mathbf{R}^i + \mathbf{X}^i \tag{6}$$

where $\mathbf{R}^i$ is the global position vector of the origin of the body coordinate system, and $\mathbf{X}^i = \begin{bmatrix} X^i & Y^i & Z^i \end{bmatrix}$ are the body parameterization. Therefore, the position vector gradients for all the elements over the body i can be obtained as

$$\frac{\partial \mathbf{r}^{ij}}{\partial \mathbf{X}^i} = \mathbf{I} \tag{7}$$

where $\mathbf{I}$ is a 3×3 identity matrix. This means that, using the **BCS**, all the position vector gradients of all elements are the same and consequently a standard ANCF assembly can be established. The gradients transformation between the **BCS** and the **ECS** can be written as[23]

$$\mathbf{r}_{\mathbf{x}^{ij}}^{ij} = \mathbf{J}_0^{ij}\mathbf{r}_{\mathbf{X}^i}^{ij} \tag{8}$$

where $\mathbf{r}_{\mathbf{x}^{ij}}^{ij} = \begin{bmatrix} r_{x^{ij}}^{ij} & r_{y^{ij}}^{ij} & r_{z^{ij}}^{ij} \end{bmatrix}^T$, $\mathbf{r}_{\mathbf{X}^i}^{ij} = \begin{bmatrix} r_{X^i}^{ij} & r_{Y^i}^{ij} & r_{Z^i}^{ij} \end{bmatrix}^T$, and

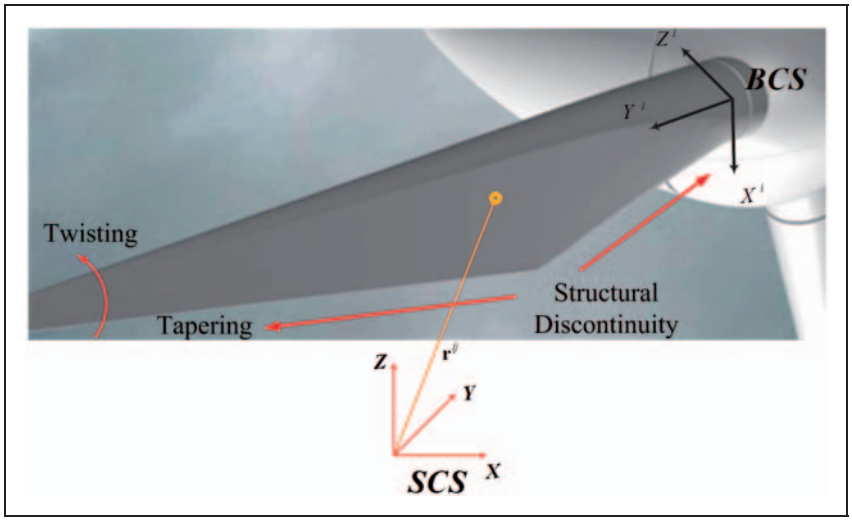

Figure 4. Structure (SCS), body (BCS), and element (ECS) coordinate systems of discontinuous structure.

$\mathbf{J}_0^{ij}$ is the orthogonal transformation matrix that describes the initial orientation of the **ECS** with respect to **BCS** and can be written in the form of

$$\mathbf{J}_0^{ij} = \begin{bmatrix} \frac{\partial X^i}{\partial x^{ij}} & \frac{\partial Y^i}{\partial x^{ij}} & \frac{\partial Z^i}{\partial x^{ij}} \\ \frac{\partial X^i}{\partial y^{ij}} & \frac{\partial Y^i}{\partial y^{ij}} & \frac{\partial Z^i}{\partial y^{ij}} \\ \frac{\partial X^i}{\partial z^{ij}} & \frac{\partial Y^i}{\partial z^{ij}} & \frac{\partial Z^i}{\partial z^{ij}} \end{bmatrix} = \begin{bmatrix} J^{ij}_{0(1,1)} & J^{ij}_{0(1,2)} & J^{ij}_{0(1,3)} \\ J^{ij}_{0(2,1)} & J^{ij}_{0(2,2)} & J^{ij}_{0(2,3)} \\ J^{ij}_{0(3,1)} & J^{ij}_{0(3,2)} & J^{ij}_{0(3,3)} \end{bmatrix} \tag{9}$$

As shown in Figure (4), slope discontinuities refer to different gradients at nodes along the elements' interface. In order to model this type of discontinuities, a coordinate transformation should be employed to attain constant mass matrix of element that undergoes finite rotation and large deformation. In this case, the element coordinate transformation at nodal point k can be carried out using the following equations

$$\mathbf{e}^{ijk} = \mathbf{T}^{ijk}\mathbf{P}^{ijk} \tag{10}$$

where $\mathbf{e}^{ijk} = \begin{bmatrix} \mathbf{r}^{ijk} & \mathbf{r}_x^{ijkT} & \mathbf{r}_y^{ijkT} & \mathbf{r}_z^{ijkT} \end{bmatrix}^T$, $\mathbf{P}^{ijk} = \begin{bmatrix} \mathbf{r}^{ijk} & \mathbf{r}_X^{ijkT} & \mathbf{r}_Y^{ijkT} & \mathbf{r}_Z^{ijkT} \end{bmatrix}^T$, and the transformation matrix $\mathbf{T}^{ijk}$ can be expressed as

$$\mathbf{T}^{ijk} = \begin{bmatrix} \mathbf{I} & \mathbf{0} & \mathbf{0} & \mathbf{0} \\ \mathbf{0} & J^{ijk}_{0(1,1)}\mathbf{I} & J^{ijk}_{0(2,1)}\mathbf{I} & J^{ijk}_{0(3,1)}\mathbf{I} \\ \mathbf{0} & J^{ijk}_{0(1,2)}\mathbf{I} & J^{ijk}_{0(2,2)}\mathbf{I} & J^{ijk}_{0(3,2)}\mathbf{I} \\ \mathbf{0} & J^{ijk}_{0(1,3)}\mathbf{I} & J^{ijk}_{0(2,3)}\mathbf{I} & J^{ijk}_{0(3,3)}\mathbf{I} \end{bmatrix} \tag{11}$$

Thus, equation (3) can be modified into

$$\mathbf{r}^{ij} = \mathbf{S}^{ij}\mathbf{T}^{ij}\mathbf{B}_1^{ij}\mathbf{B}_2^{i}\mathbf{P}^{i} \tag{12}$$

This allows maintaining the ANCF desirable features that include a constant mass matrix and zero Coriolis and centrifugal forces in the equations of motion of structures that experience arbitrary large displacements. For gradient-deficient ANCF finite elements as in the case of thin plates, equation (10) reduces to[23]

$$\begin{bmatrix} \mathbf{r}^{ijk} \\ \mathbf{r}_{x^{ij}}^{ijk} \\ \mathbf{r}_{y^{ij}}^{ijk} \end{bmatrix} = \begin{bmatrix} \mathbf{I} & \mathbf{0} & \mathbf{0} & \mathbf{0} \\ \mathbf{0} & J^{ijk}_{0(1,1)}\mathbf{I} & J^{ijk}_{0(2,1)}\mathbf{I} & J^{ijk}_{0(3,1)}\mathbf{I} \\ \mathbf{0} & J^{ijk}_{0(1,2)}\mathbf{I} & J^{ijk}_{0(2,2)}\mathbf{I} & J^{ijk}_{0(3,2)}\mathbf{I} \end{bmatrix} \begin{bmatrix} \mathbf{r}^{ijk} \\ \mathbf{r}_X^{ijk} \\ \mathbf{r}_Y^{ijk} \\ \mathbf{r}_Z^{ijk} \end{bmatrix} \tag{13}$$

The use of thin plate element in modeling the wind turbine plate is obvious because of the large relative size between the plate thickness and the plate length and width. Structural discontinuity in this case is apparent along the blade length, and therefore equation (13) should be used. Equation (13) explains the transformation between the element-parameterized gradient coordinates and the body-parameterized gradient coordinates. However, this transformation leads to a larger number of coordinates than that of the original element coordinates. Such a transformation cannot be used since it leads to redundant degrees of freedom in the resulting equations of motion. In order to avoid redundancy of nodal coordinates, it is proposed to use the lofted surface geometry to model the structural discontinuities of wind turbine blade, and this method is illustrated in the following subsection.

Modeling slope discontinuity

Structural discontinuities are found in two places of the wind turbine blade structure. The first place lies in the interface section between the upper and lower

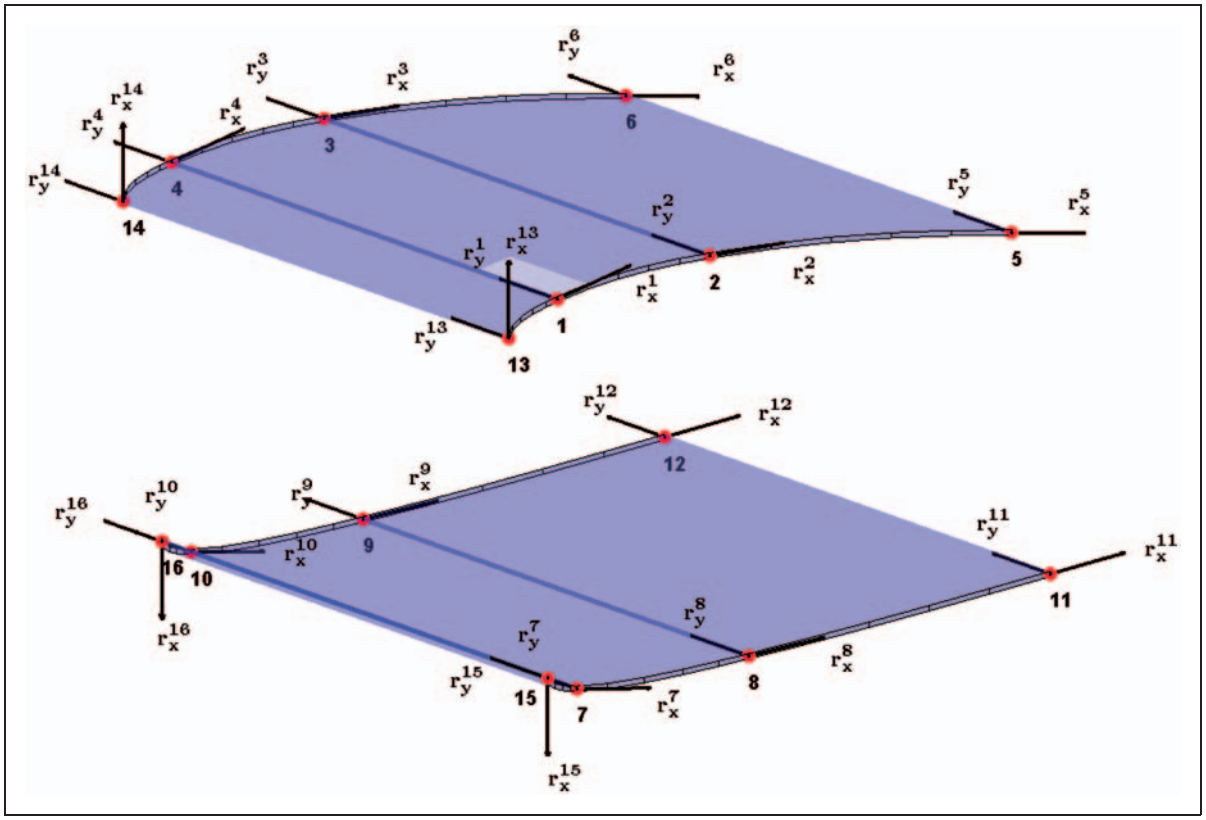

Figure 5. ANCF model for upper and lower surfaces of uniform blade section.

surfaces, see Figure 5. These surfaces are generated directly from the NACA code thickness distribution,[18] and this case is denoted as chord-wise slope discontinuity. The second place in the interface between the blade-root and the blade-span sections, see Figure 4, and this structural discontinuity is denoted as span-wise slope discontinuity.

The chord-wise slope discontinuity can be modeled with reasonable accuracy using fillets which can be introduced systematically using initially curved elements. Fillet can be used and curved plate elements can be constructed. By the fillets constructed in the leading and trailing edges, a continuous structure ANCF model can be obtained. These fillets cancel four nodes, which have the discontinuous gradients, see Figure 6.

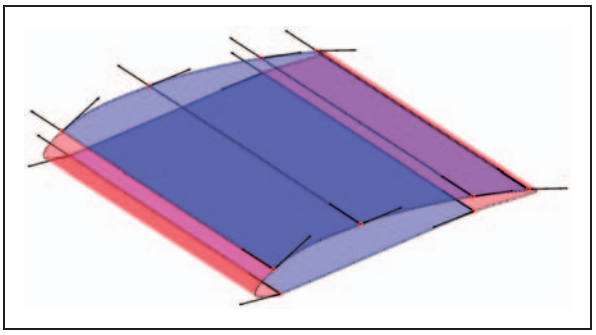

Figure 6. Modeling of chord-wise slope discontinuity at leading/trailing edges.

In the case of modeling span-wise slope discontinuity, lofted surface is constructed along the blade length, particularly between the 'start' and the 'tip' cross and between the 'start' and 'root' sectional curves, see Figure 9. In the case of obtaining the global position vector for the non-uniform wind turbine blade, the position vector $\mathbf{r}$ should be linearly interpolated between the blade starting-chord, c_1, and tip-chord c_2. This bounded curves can be denoted by $\mathbf{r}(\xi, 0)$ and $\mathbf{r}(\xi, 1)$ and by two straight segments $\mathbf{r}(0, \eta)$ and $\mathbf{r}(1, \eta)$ connecting them. Surface lines in η direction are therefore straight, i.e. lofted surfaces,[24] whereas each line in the ξ direction is a blend of $\mathbf{r}(\xi, 0)$ and $\mathbf{r}(\xi, 1)$, and this blend constitutes the surface expression of

$$\mathbf{r}(\xi, \eta) = (1 - \eta)\mathbf{r}(\xi, 0) + \eta\,\mathbf{r}(\xi, 1) \tag{14}$$

where η and ξ are parametric domains such that $\xi, \eta \in [0, 1]$ and can be estimated as $\xi = x/a$, $\eta = y/b$, where a and b are the plate element length and width, respectively. It should be mentioned here that this kind of surface is fully defined by specifying the two boundary curves. A similar procedure can be carried out to construct the blade-root section. The start cross-section of the blade is used with the

circular edge of the root surface to construct the lofting surface between them. The boundary curves can be written as

$$\mathbf{r}(\xi,0)=\mathbf{r}^i=\mathbf{S}(x,0)\mathbf{e}\cdots,x\in[0,c_1] \tag{15}$$

where $\mathbf{e}$ is the nodal coordinates along the curve of the starting-chord, curve i. Thus, the position vector of an arbitrary point along the tip curve, curve j, can be concluded as

$$\mathbf{r}(\xi,1)=\mathbf{r}^j=\begin{bmatrix}0\\L_s\\0\end{bmatrix}+\begin{bmatrix}\frac{c_2}{c_1}&0&0\\0&1&0\\0&0&\frac{c_2}{c_1}\end{bmatrix}\mathbf{r}(\xi,0)\cdots,x\in[0,c_2] \tag{16}$$

whereas the position vector of an arbitrary point along the circular root curve, curve k, can be obtained as

$$\mathbf{r}(\xi,1)=\mathbf{r}^k=\begin{bmatrix}0\\-L_r\\0\end{bmatrix}+\begin{bmatrix}\cos\theta&0&0\\0&0&0\\0&0&\sin\theta\end{bmatrix}\times c_r\cdots,\theta\in[0,2\pi] \tag{17}$$

such that c_1, c_2, and c_r are the chord lengths at the starting, tip, and root sections along the blade. Simply c_r is the radius of the circular curve of the blade-root. L_s and L_r are the blade-span and blade-root lengths, such that the total length of the blade is L_s+L_r. Substituting equationd (15) and (16) into equation (14) gives the lofted surfaces between $\mathbf{r}^i$ and $\mathbf{r}^j$, which can be solved for the nodal positions at the tip curve. Also, substituting equationd (15) and (17) into equation (14) gives the lofted surfaces between $\mathbf{r}^i$ and $\mathbf{r}^k$, which can be solved for the nodal positions at the circular root curve. The span-wise slope discontinuity can be modeled by using the lofting equation for the gradients transformation as well as the nodal position transformation. The gradients of the lofted surface can be obtained as

$$\frac{d\mathbf{r}(\xi,\eta)}{\mathrm{d}\xi}=(1-\eta)\frac{d\mathbf{S}(\xi,0)}{\mathrm{d}\xi}\mathbf{e}+\eta\frac{d\mathbf{S}(\xi,1)}{\mathrm{d}\xi}\mathbf{e} \tag{18}$$

$$\frac{d\mathbf{r}(\xi,\eta)}{\mathrm{d}\eta}=-\mathbf{r}(\xi,0)+\mathbf{r}(\xi,1) \tag{19}$$

It is therefore possible to obtain the nodal positions and gradients necessary to construct the ANCF model of a complete blade structure; see Figure 7 for the blade-span section and Figure 8 for the blade-root section. It is necessary to emphasise that using equationd (18) and (19), a continuous ANCF model can be obtained for the structure of large size wind turbine blade, see Figure 9. By using equations (18) and (19) to calculate the gradients of lofted surface; equation (13) is reduced to identity matrix, and therefore the desirable features of the ANCF can be maintained.

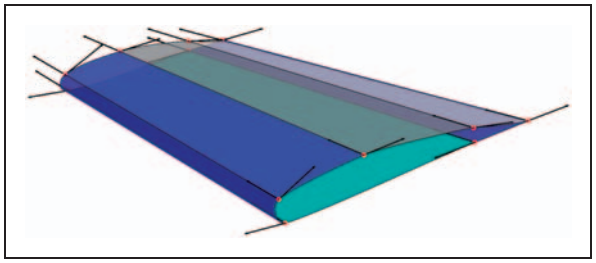

Figure 7. Lofted surfaces of the blade-span section.

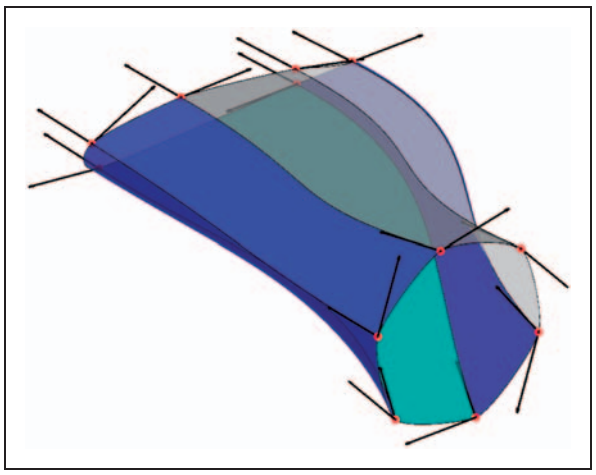

Figure 8. Lofted surfaces of the blade-root section.

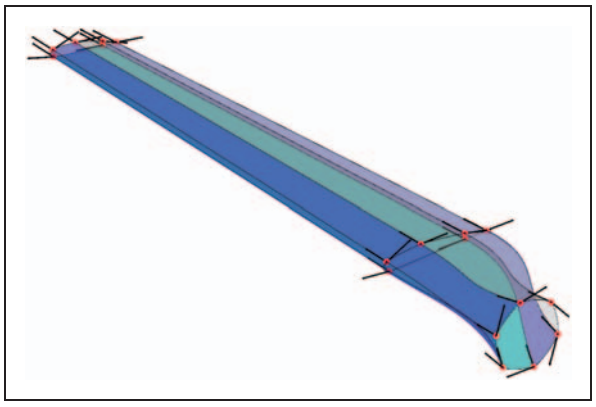

Figure 9. Continuous ANCF model of large size wind turbine blade.

Equations of motions and solution methods

Once the geometric representation of the blade model is obtained, and using the element mass matrix, $\mathbf{M}^i$

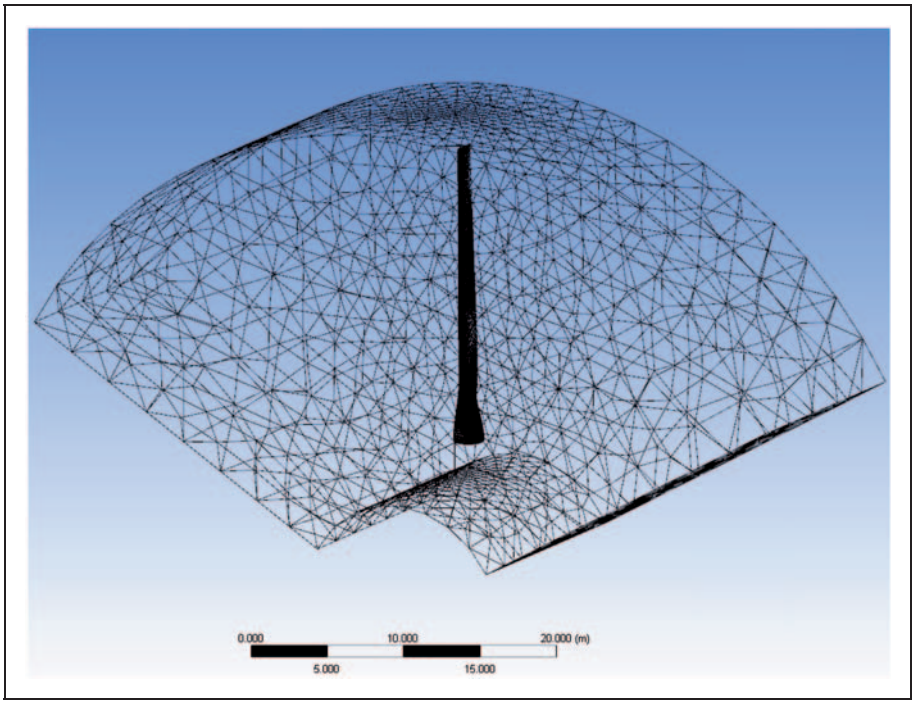

Figure 10. Fluid domain mesh.

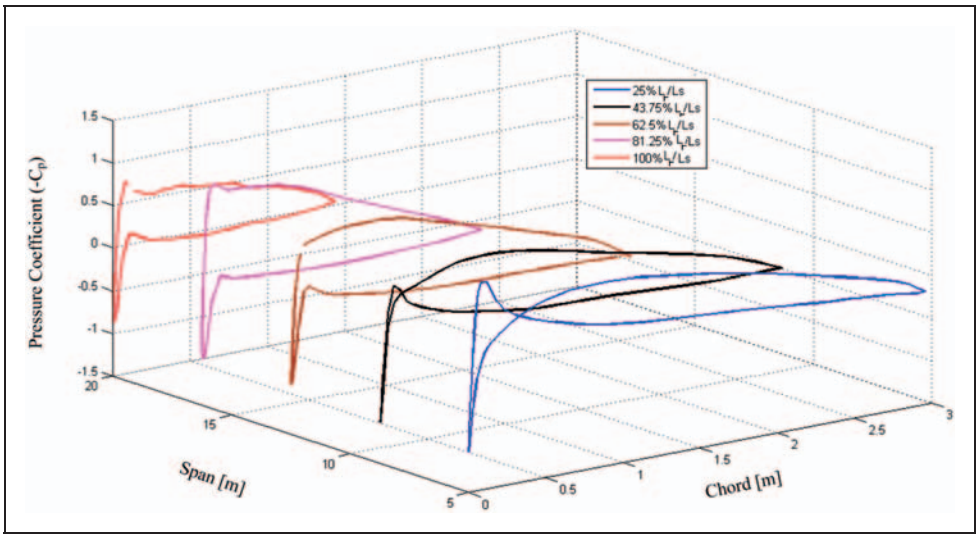

Figure 11. Pressure coefficient distribution along the blade.

and the elastic force vector, $\mathbf{Q}_k^i$,[18] the equations of motion of the body i can be written as

$$\mathbf{M}^i\ddot{\mathbf{P}}^i + \mathbf{Q}_k^i = \mathbf{Q}_e^i \tag{20}$$

where $\mathbf{Q}_e^i$ is generalized force vector corresponding to aerodynamic forces and gravity forces. These vectors are simplified in Bayoumy et al.[18] by using approximate expressions of left and drag coefficients. Particularly, the aerodynamic forces are generated due to fluid–solid interaction between the blade and the wind. The resulted pressure distribution along the blade due to the wind speed is dependent on the wind speed as well as the blade geometry. It is therefore necessary to define the fluid domain around the rotor blade and estimate the pressure coefficient $C_p(x, y)$. Hence, the pressure distribution, $P^{ij}(x, y)$, along the element j on the body i and the corresponding element force, $\mathbf{F}^{ij}$, can be written as[1,25]

$$P^{ij}(x, y) = -0.5\rho v^2 C_p^{ij}(x, y)\mathbf{n}^{ij} \tag{21}$$

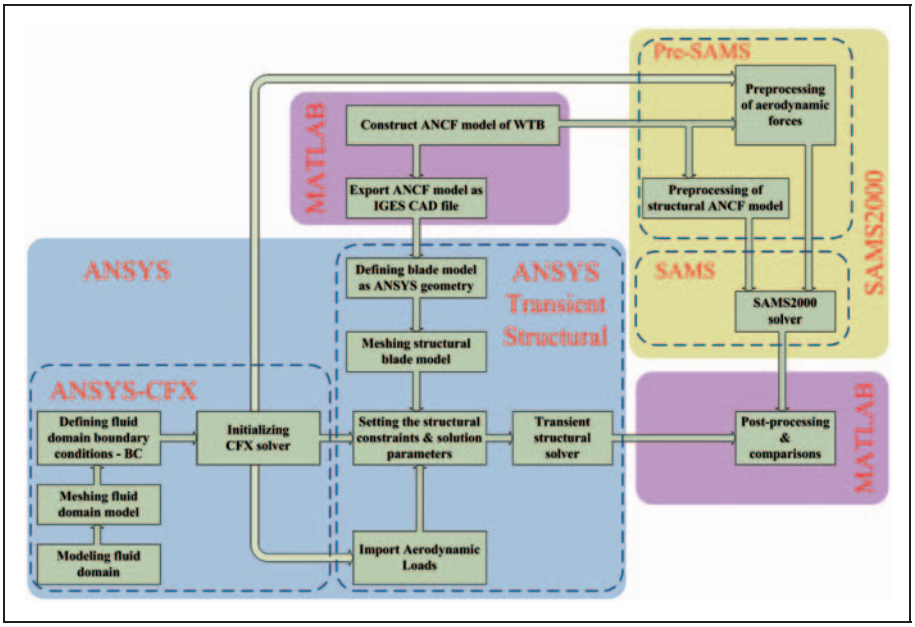

Figure 12. Forward dynamics scheme.

Figure 13. An example of static load test: Glasfiber Blade Test, LM 61.5 m blade. http://www.wind-energy-the-facts.org/en/part-i-technology/chapter-3-wind-turbine-technology/current-developments

Table 1. Static tip-deformation of wind blade.

#	Position from root (m)	Applied load (KN)	ANCF Tip deflection (m)	ANSYS Tip deflection (m)
I	5	0.116		
	10	0.116	1.358	1.4257
	15	0.116		
II	5	0.33		
	10	0.33	4.537	Non-convergent
	15	0.33		
III	5	3.33		
	10	3.33	15.68	Non-convergent
	15	3.33		

$$\mathbf{F}^{ij} = \int_{A^{ij}} P^{ij}(x,y)\mathrm{d}A^{ij} \tag{22}$$

where ρ is the air density, v is the wind speed and $\mathbf{n}^{ij}$ is the normal vector over the element surface. The generalized force vector corresponding to the absolute nodal coordinates, $\mathbf{Q}_e^{ij}$, can be estimated as

$$\mathbf{Q}_e^{ij} = \int_{V_0^{ij}} \mathbf{S}^{ijT}\mathbf{F}^{ij}\mathrm{d}V_0^{ij} \tag{23}$$

It is clear from equation (21) that $C_p^{ij}(x,y)$ is the key parameter for estimating the aerodynamic forces affecting the blade. In this investigation, given the blade model and its CAD representation, the ANSYS-CFX module[26] is used to estimate of the power coefficient along the blade. These values of power coefficients should be integrated in the equations of motion based on equation (20).

The ANCF model is constructed using the MATLAB.[27] The obtained nodal coordinates and elements properties are fed forward to SAMS software[28] for solving equation (20). Also, the

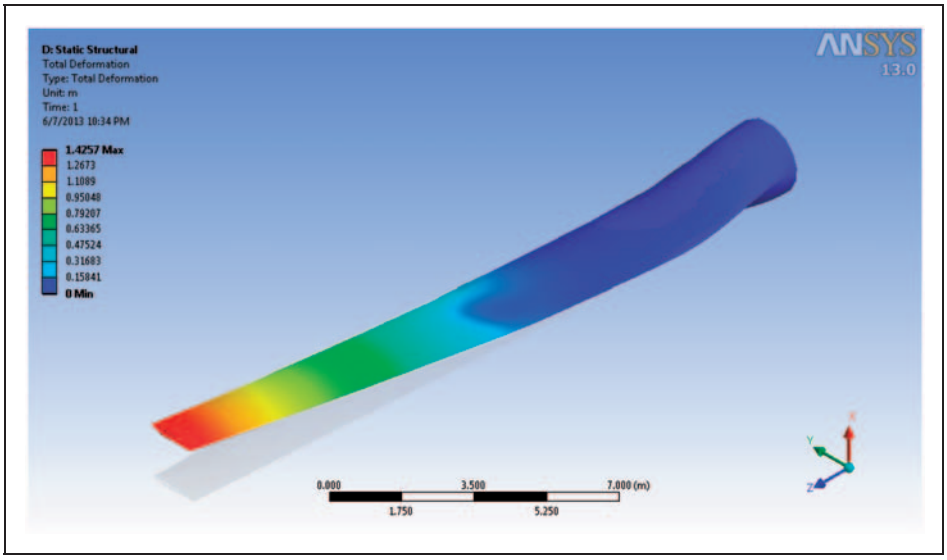

Figure 14. Static solution of blade model using ANSYS (Test I).

corresponding CAD model is extracted and fed forward to ANSYS-CFX module[26] to obtain the power coefficients along the blade. Figures 10 and 11 show an example to use the ANSYS-CFX module to generate the power coefficients distribution along 25 m wind blade. This example is carried out with the following values: NACA 4412 profile, blade-span length $L_s = 20[m]$, blade-root length $L_r = 5[m]$, root radius $c_r = 1[m]$, taper angle of 6°, twist angle of 10°, chord length at the blade start-section $c_1 = 3[m]$. The fluid domain around the rotor blade is divided into one-third of the fluid domain circle that encloses the whole turbine diameter, see Figure 10. The boundary conditions are considered to have inlet air velocity of 5.1 m/s, at 25°C, i.e. the horizontal component 5 m/s and the vertical component 1 m/s. Figure 11 shows the resulted pressure coefficient distribution at certain locations along the blade. It can be noticed that the pressure differential across the blade lower/upper sides increases along the span length which increases the aerodynamic lift forces and consequently the deflection of the blade increases toward its tip.

The forward dynamic scheme then can be summarized as shown in Figure 12. The procedure dynamics simulation of large size wind turbine blades can be carried out using the following stages:

Stage A: ANSYS-CFX (Analysis System Software, ANSYS, Inc.)

1. The fluid domain is constructed and the boundary conditions are defined.
2. The meshing of the fluid domain is generated.
3. The aerodynamics loads are generated by running the CFX solver corresponding to the fluid domain in stage A.1. to give the pressure coefficient distribution.

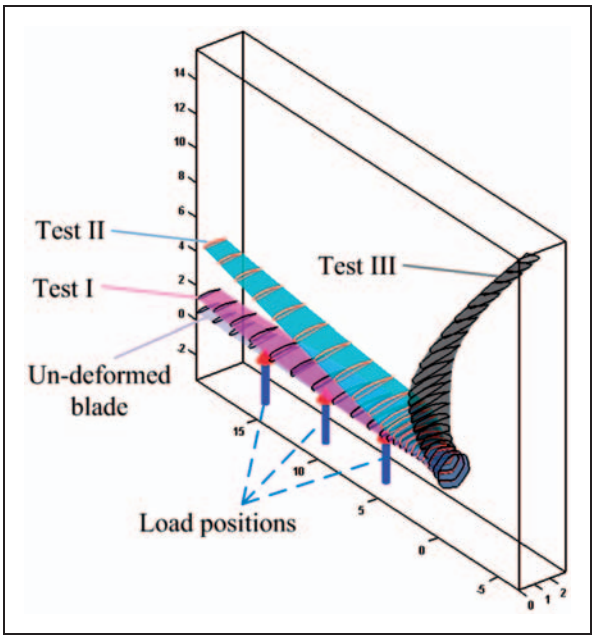

Figure 15. Static solution of ANCF blade model (Tests I, II, and III).

Stage B: MATLAB (Matrix Laboratory, Mathworks, Inc.)

1. The ANCF model, i.e. nodes and gradients of wind blade are calculated as described in the ANCF model of wind turbine blades section.
2. The generated ANCF model is exported to IGES CAD (Computer Aided Design file format file).
3. The generalized force vector is estimated based on the output of stage A.3. based on equation (23).

Stage C: SAMS (Systematic Analysis of Multibody Systems, Textbook accompanying software)[28]

1. The ANCF input data file (PRESAMS-file) is generated for the model constructed in stage B.1.
2. The USER Subroutine of aerodynamics loads (stage A.3.) is constructed as generalized forces (SAMS USER FUNCTION).
3. The dynamic simulation is carried out using SAMS solver.

Stage D: ANSYS transient structural module

1. Define the blade model generated in stage B.2. as ANSYS geometry.
2. The meshing of the structural blade model is generated.
3. Define structural constraints of the blade model.
4. Import the aerodynamic loads generated in Stage A.3.
5. The dynamic simulation is carried out using ANSYS-Transient Structural Module solver.

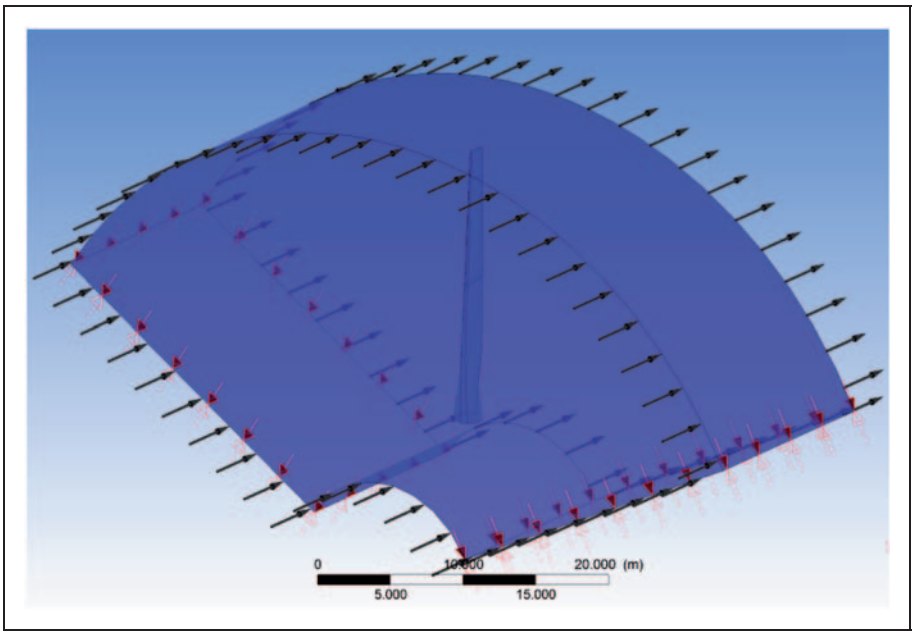

Figure 16. Mesh boundary conditions (normal condition: twist angle 10°).

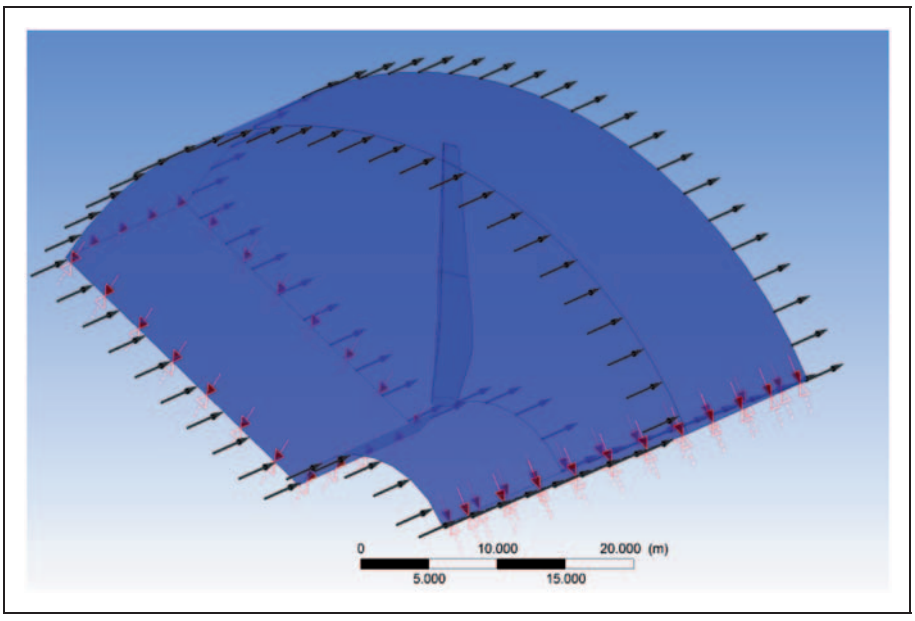

Figure 17. Mesh boundary conditions (full-feathered condition: twist angle 90°).

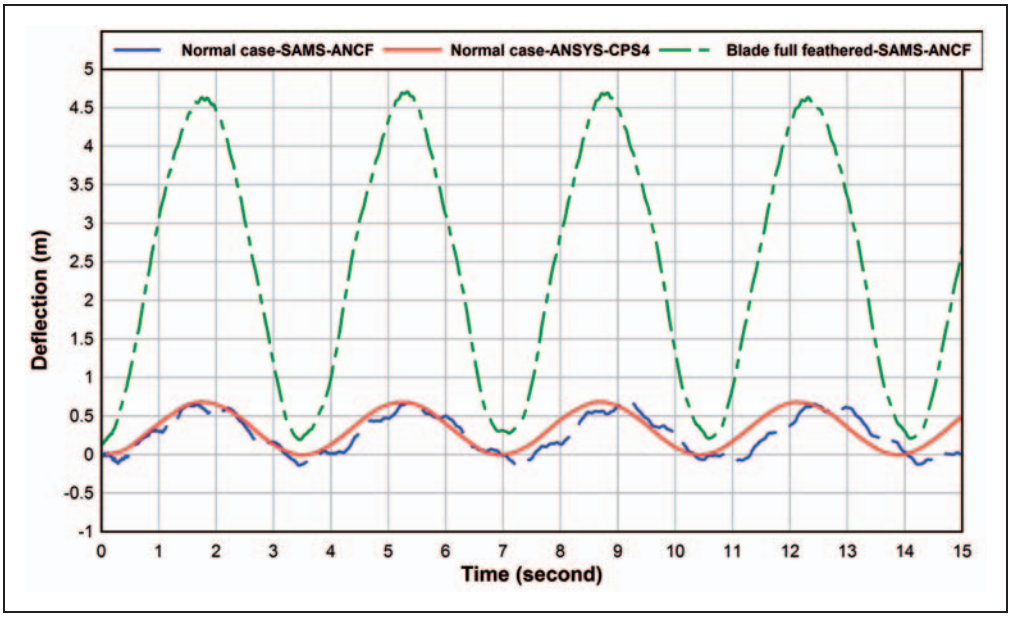

Figure 18. Dynamic simulation due to aerodynamic loads.

The post-processing of the results, Stages C.3 and D.5, are carried out and the dynamic characteristics are compared to each other, see Figure 12.

Static loading test

In the static test, which is required as part of blade certification, the blade is pulled in the horizontal or vertical axis, flap-wise, in order to measure blade deflection. Static testing will be performed with a combination of computer-controlled servo-hydraulic winches and cylinders connected through cables to the blade, see Figure 13. The ultimate static test is carried out by pulling a blade to failure point. In this subsection, three static tests will be investigated to express the advantages of use the ANCF in modeling large size wind turbine blades. In ANSYS, the static analysis can be performed by replacing the transient-structural module by statics-structural module. However, in the ANCF, the solution is carried out by setting the generalized acceleration vector as zero vector and thereby, $Q = 0$; the result is obtained using the Newton-Raphson method.

In ANSYS, the plane-stress 4-node bilinear element is used in meshing the structural model of the blade. In ANCF model, 12-thin plate elements are used along the blade. Table 1 illustrates the load values and its positions as well as the transverse deformation of the tip point. In this particular case, ANSYS did not converge to solution for both the second and third test, even with using large deflection analysis option. However, ANCF model solution converges due to its suitability to solve the

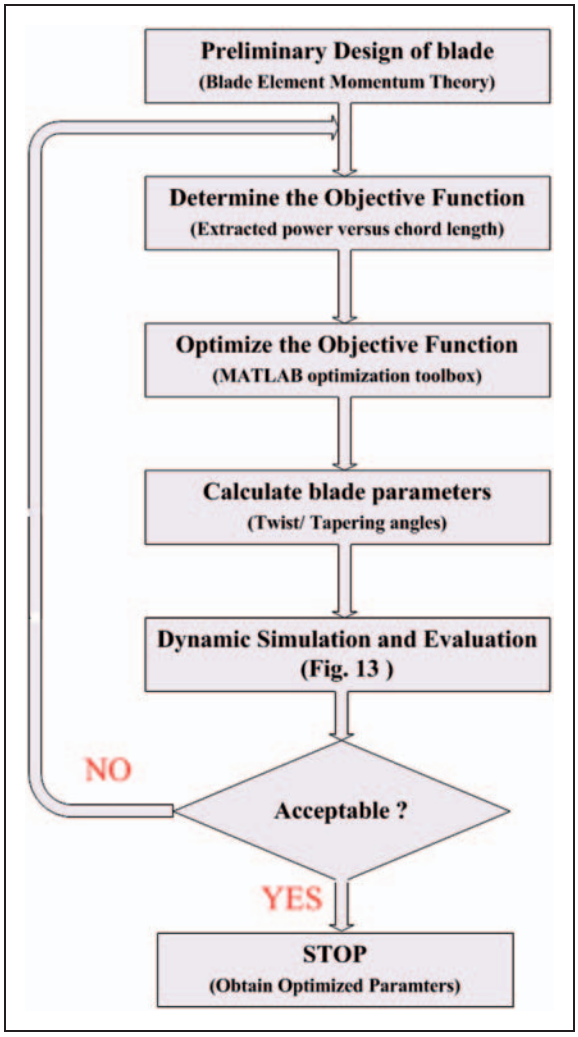

Figure 19. Dynamics for design procedure.

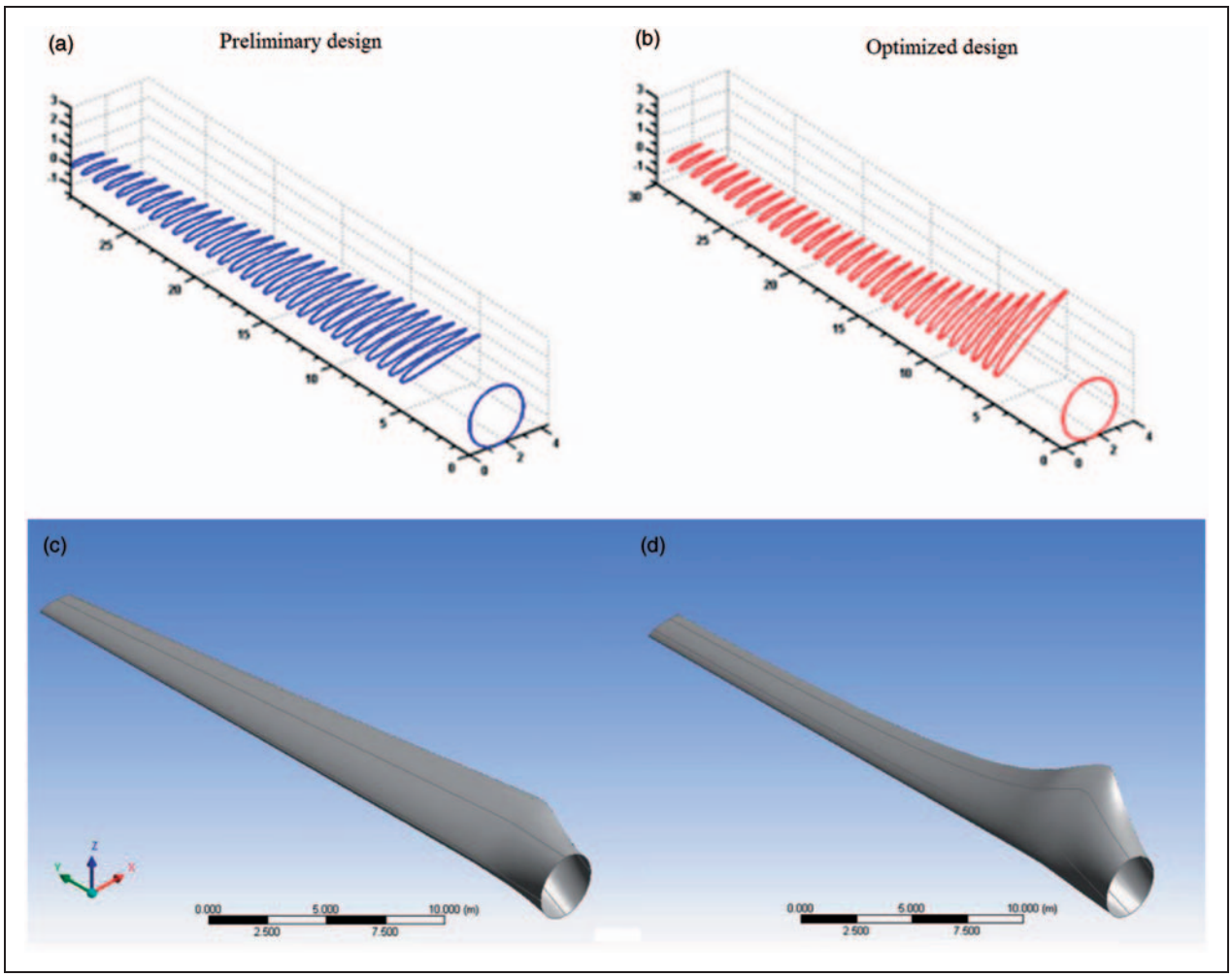

Figure 20. Preliminary versus optimized design.

large deformation problems for very flexible structures. Figure 14 shows the static solution of test *I* using ANSYS, and it is shown that the static deflection of the tip point is 1.4257 m. The value obtained with the ANCF model is 1.358 m as listed in Table 1. The ANCF gives a transverse deflection of 4.537 and 15.68 m for tests *II* and *III* respectively, see Figure 15.

Dynamic analysis

In order to examine the effectiveness of the ANCF model, the dynamic simulation of a full-feathered blade is examined. Feathering the blades means to increase their pitch angle by turning the blades to the perpendicular direction of the airflow. In this case, the rotational speed is minimized and the lift force is increased and therefore it results in large deformation of the blade in the transverse direction. According to the dynamic simulation stage A.2., the fluid domain is generated around the blade, see Figure 10. The aerodynamic loads are generated and applied upon the normal condition (twist angle of 10°), see Figure 16 and full-feathered condition (twist angle of 90°), see Figure 17. The generalized forces of the aerodynamic loads are constructed according to stage B.3.

The time integration methods used particularly in this investigation are based on the Newmark method.[12,20] In ANSYS, the Newmark integration method is used with sparse direct solver for stabilization process. Applying the Newmark method results in a linear system of equation for each time step, automatic time stepping is available, all kinds of loads may be specified, and masses are not assumed to be concentrated at the nodes. The main disadvantage is that large disk or in-core memory requirements should be available.

In SAMS, two-loop implicit sparse matrix numerical integration is used, in which the algebraic constraint equations are satisfied at all levels, and does not require the numerical differentiation of the forces. This method is used with the HHT implicit integration formulas, which contain numerical damping that can be adjusted to damp out high frequency ANCF coupled deformation modes. While implicit integration methods include numerical damping that can filter out the contributions of fundamental modes of

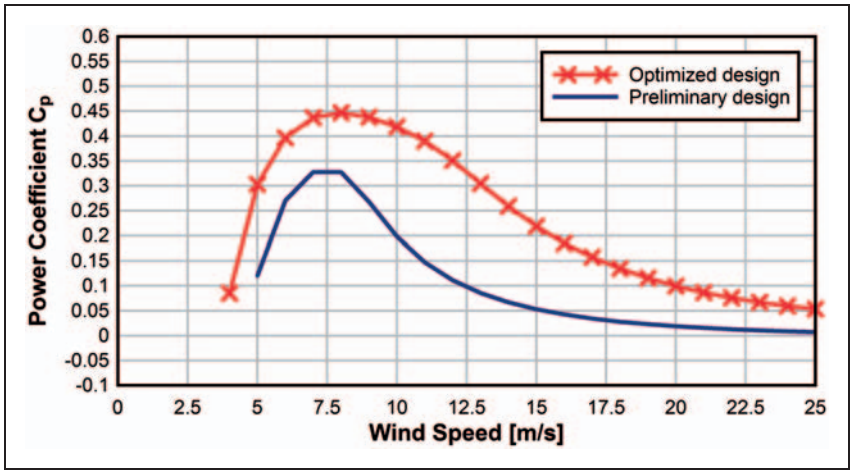

Figure 21. Comparison of power coefficients.

deformations, the two-loop implicit sparse matrix numerical integration, on the other hand, captures the contributions of these fundamental modes.[13] HHT-Sparse integration is used with a time interval of 1 ms, relative and absolute errors of 1×10^{-6}.

Figure 18 shows the dynamic simulation of the wind turbine blade due to aerodynamic wind stream of 5 m/s upon two conditions (normal/full-feathered), see Table 2 in Appendix 1 for the blade specification. It is shown that the dynamic characteristics obtained using ANSYS/ANCF models are close to each other, in both amplitude and frequency in the normal operating condition. However, in the full-feathered conditions, ANSYS solver failed to capture the dynamic solution. ANCF model, which is suited for large rotation large deformation problems, gives the dynamic solution as shown in Figure 18. One of the advantages of using the ANCF in modeling large size wind turbine blades is the ability to capture the high frequency modes and therefore compensate the numerical errors.

Layout of dynamics for design procedure

The dynamic modeling of large size wind turbine blades using the ANCF can improve the design process of such blades. The dynamic characteristics help to predict the dynamic loading capacity and energy losses. These two factors affect, in turns, on the rotor torque, the output power and consequently the blade efficiency.

The procedure of designing the wind turbine blade using the obtained dynamic model is summarized in Figure 19.The preliminary design is obtained based on the blade element momentum theory,[1,25,29,30] and the objective function is then built relating the tip-speed ratio with the preliminary design parameters. In this work, single variable optimization is carried out; the chord length is optimized with respect to the extracted power, and the other blade parameters (twist angle, tapering angles) are concluded. Once the blade model is constructed, the dynamic simulation is carried out and the dynamic characteristics are evaluated. Several try and error iterations are carried out to enhance the aerodynamic performance of the wind turbine blade. An example for enhancing the design of the blade, using the proposed procedure, is illustrated in Figure 20. It is clear that the blade shape is optimized by lighting the aerodynamic section (blade-span) and strengthening the structural section (blade-root) of the blade. A comparison between the power coefficients of preliminary and optimized shapes is shown in Figure 21.

Summary and conclusions

In this paper, an efficient procedure is developed for mapping NACA airfoil wind turbine blades into ANCF thin plate models. The procedure concerned a complete aerodynamic/structural blade model with the non-uniform and twisted configuration. The structural slope discontinuity due to variations of the cross-sectional layouts across the blade is manipulated successfully to avoid the computational redundancy due to gradient transformation. The chord-wise slope discontinuity is modelled with reasonable accuracy using fillets which can be introduced systematically using initially curved elements. However, the span-wise slope discontinuity is modelled by using the lofted surface geometry. The effectiveness of using ANCF in modeling large size wind turbine blades is examined through dynamic/static simulation procedure. Several numerical examples are solved and ensure the ability of obtaining convergent solutions for large rotation and large deformation operating conditions. It is found that one advantage of using ANCF in modeling large size wind turbine blade is the ability to capture high frequency modes and overcome the geometric stiffness effect. As a result, a layout of dynamics-for-design procedure is constructed and examined in optimizing the blade shape for enhancing the aerodynamic performance. Several key points should be concerned and studied in future

studies, such as efficiency of using thick plate element and new gradient-deficient spatial curved beam and cylindrical shell elements in ANCF, also adding the curvature vector at the nodes in order to allow for the description of the cross section deformation in case of fibre.

Funding

This research received no specific grant from any funding agency in the public, commercial, or not-for-profit sectors.

References

1. Hansen MOL. *Aerodynamics of wind turbines*. 2nd ed. London: Earthscan, 2008.
2. Kalleoe BS. *Aeroservoelasticity of wind turbines*. PhD thesis, Dept. of Mechanical Engineering, Technical University of Denmark.
3. Chandler H. *Wind energy: the facts: an analysis of wind energy in the EU-25*. Brussels, Belgium: European Wind Energy Association, 2004.
4. http://en.wikipedia.org/wiki/Enercon_E-126#cite_note-0.
5. Schubel PJ and Crossley RJ. Wind turbine blade design. *Energies* 2012; 5: 3425–3449.
6. Hansena MOL, Srensena JN, Voutsinasb S, et al. State of the art in wind turbine aerodynamics and aeroelasticity. *Aerospace Sci* 2006; 42: 285–330.
7. Hussein BA, Sugiyama H and Shabana AA. Coupled deformation modes in the finite element absolute nodal coordinate formulation. In: *12th IFToMM World Congress*. Besançon, France, 18–21 June 2007.
8. Nada AA. Use of B-spline surface to model large-deformation continuum plates: procedure and applications. *Nonlinear Dynam* 2013; 72: 243–263.
9. Nada AA, Hussein BA, Megahed SM, et al. Use of the floating frame of reference formulation in large deformation analysis: experimental and numerical validation. *Proc IMechE, Part K: J Multi-body Dynamics* 2010; 224: 45–58.
10. Garcia-Vallejo D, Mayo J, Escalona JL, et al. Efficient evaluation of the elastic forces and the Jacobian in the absolute nodal coordinate formulation. *Nonlinear Dynam* 2004; 35: 313–329.
11. Dmitrochenko ON, Hussein BA and Shabana AA. Coupled deformation modes in the large deformation finite element analysis: generalization. *J Computat Nonlinear Dynam* 2009; 4: 8.
12. Hussein BA, Negrut D and Shabana AA. Implicit and explicit integration in the solution of the absolute nodal coordinate differential/algebraic equations. *Nonlinear Dynam* 2008; 54: 283–296.
13. Hussein BA and Shabana AA. Sparse matrix implicit numerical integration of the Stiff differential/algebraic equations: Implementation. *Nonlinear Dynam* 2011; 65: 369–382.
14. Sugiyama H, Escalona J and Shabana AA. Formulation of three-dimensional joint constraints using the absolute nodal coordinates. *Nonlinear Dynam* 2003; 31: 167–195.
15. Garcia-Vallejo D, Valverde J and Dominguez J. An internal damping model for the absolute nodal coordinate formulation. *Nonlinear Dynam* 2005; 42: 347–369.
16. Abdel-Nasser M and Shabana AA. A nonlinear visco-elastic constitutive model for large rotation finite element formulations. *Multibody Syst Dynam* 2011; 26: 57–79.
17. Nada AA and El-Assal AM. Absolute nodal coordinate formulation of large-deformation piezoelectric laminated plates. *Nonlinear Dynam* 2012; 67: 2241–2454.
18. Bayoumy AH, Nada AA and Megahed SM. A continuum based three-dimensional modeling of wind turbine blades. *J Computat Nonlinear Dynam* 2013; 8: 031004 (14 p).
19. Bayoumy AH, Nada AA and Megahed SM. Modeling slope discontinuity of large size wind-turbine blade using absolute nodal coordinate formulation. In: *Proceedings of the ASME 2012 international design engineering technical conferences &computers and information in engineering conference (IDETC/CIE 2012)*. Chicago, IL, 12–15 August 2012.
20. *ANSYS User's Manual, Theory*. 12th ed. Canonsburg: SAS IP, 2001.
21. Shabana AA. *Computational continuum mechanics*. Cambridge, UK: Cambridge University Press, 2010.
22. Shabana AA and Mikkola AM. Use of the finite element absolute nodal coordinate formulation in modeling slope discontinuity. *J Mech Des* 2003; 125: 342–350.
23. Shabana AA. General method for modeling slope discontinuities and T-Sections using ANCF gradient deficient finite elements. *J Computat Nonlinear Dynam* 2011; 6: 024502.
24. Gerlad F. *Curves and surfaces for CAGD: a practical guide*. 5th ed. San Francisco, CA, USA: Morgan Kaufmann Publishers, 2001.
25. Dong-Hyun K and Yoo-Han K. Performance prediction of a 5MW wind turbine blade considering aeroelastic effect. *World Acad Sci Eng Technol* 2011; 57: 698–702.
26. *ANSYS CFD-Post User's Guide*. http://www.ansys.comANSYS, Inc, 2001.
27. MATLAB Release 2012bwww.mathworks.com
28. Shabana AA. *Computational dynamics*. 3rd ed. Wiley, 2010.
29. Hua X, Rui GU, Jin J, et al. Numerical simulation and aerodynamic performance comparison between Seagull aerofoil and NACA 4412 aerofoil under low-Reynolds. *Adv Nat Sci* 2010; 3: 244.
30. Rajakumar S and Ravindran D. Computational fluid dynamics of wind turbine blade at various angles of attack and low Reynolds number. *Int J Eng Sci Technol* 2010; 2: 6474–6484.

Appendix 1: Blade specification

Table 2. Specifications of the wind turbine blade used in dynamics simulation.

NACA Code	4412
Blade-span length	$L_s = 20$ m
Blade-root length	$L_r = 5$ m
Root radius	$c_r = 1.5$ m
Plate thickness	$t = 0.02$ m
Taper angle	$\alpha = 6^\circ$
Blade twist angle	$\beta = 10^\circ$
Chord length	$c_l = 1.5$ m
Modulus of elasticity	$E = 200$ MPa
Density	7050 Kg/m^3